

Article

Hybrid Artificial Intelligence Models with Multi Objective Optimization for Prediction of Tribological Behavior of Polytetrafluoroethylene Matrix Composites

Musa Alhaji Ibrahim ^{1,2,*}, Hüseyin Çamur ², Mahmut A. Savaş ², Alhassan Kawu Sabo ³, Mamunu Mustapha ⁴ and Sani I. Abba ⁵

¹ Department of Mechanical Engineering, Faculty of Engineering, Kano University of Science and Technology, Wudil P.M.B. 3244, Kano 713101, Nigeria

² Department of Mechanical Engineering, Faculty of Engineering, Near East University, via Mersin 10, Nicosia 99138, Turkey

³ Physical Planning and Development Unit, Kano University of Science and Technology, Wudil P.M.B. 3244, Kano 713101, Nigeria

⁴ Department of Electrical Engineering, Faculty of Engineering, Kano University of Science and Technology, Wudil P.M.B. 3244, Kano 713101, Nigeria

⁵ Interdisciplinary Research Center for Membrane and Water Security, King Fahd University of Petroleum and Minerals, Dhahran 31261, Saudi Arabia

* Correspondence: musaibrahim@kustwudil.edu.ng; Tel.: +234-706-921-8827



Citation: Ibrahim, M.A.; Çamur, H.; Savaş, M.A.; Sabo, A.K.; Mustapha, M.; Abba, S.I. Hybrid Artificial Intelligence Models with Multi Objective Optimization for Prediction of Tribological Behavior of Polytetrafluoroethylene Matrix Composites. *Appl. Sci.* **2022**, *12*, 8671. <https://doi.org/10.3390/app12178671>

Academic Editors: Absalom Ezugwu, Haruna Chiroma, Laith Abualigah and Roberto A. Vazquez

Received: 4 February 2022

Accepted: 3 March 2022

Published: 30 August 2022

Publisher's Note: MDPI stays neutral with regard to jurisdictional claims in published maps and institutional affiliations.



Copyright: © 2022 by the authors. Licensee MDPI, Basel, Switzerland. This article is an open access article distributed under the terms and conditions of the Creative Commons Attribution (CC BY) license (<https://creativecommons.org/licenses/by/4.0/>).

Abstract: This study presents multi-response optimization and prediction tribological behaviors polytetrafluoroethylene (PTFE) matrix composites. For multi-response optimization, the Taguchi model was hybridized with grey relational analysis to produce grey relational grades (GRG). A support vector regression (SVR) model was combined with novel Harris Hawks' optimization (HHO) and swarm particle optimization (PSO) models to form hybrid SVR-HHO and SVR-PSO models to predict the GRG. The prediction ability of the models was appraised using the coefficient of determination (R^2), correlation coefficient (R), mean square error (MSE), root mean square (RMSE), and mean absolute percentage error (MAPE). The results of the multi-response optimization revealed that the optimal combination of parametric values of GRG for minimum tribological rate was 9 N-1000 mesh-0.14 ms⁻¹-55 m (L3G1SD3SS3). An analysis of variance of the GRG showed that a grit size of 94.56% was the most significant parameter influencing the tribological behavior of PTFE matrix composites. The validation results revealed that an improvement of 52% in GRG was achieved. The prediction results of all models showed that the SVR-PSO and SVR-HHO models were superior to the SVR model. Furthermore, the SVR-HHO model produced superior prediction error and the best goodness of fit over the SVR-PSO model. These findings concluded that hybrids models are promising tools in the multi-response optimization and prediction of tribological behaviors of PTFE matrix composites. They can serve as a guide in the design and development of tribological materials.

Keywords: PTFE; bronze; carbon; tribological behaviors; Taguchi; grey relational analysis; novel AI

1. Introduction

Polymer matrix composites (PMCs) containing fibres continue to receive significant attention from industries like the automotive, aerospace, and agricultural sectors due to their improved mechanical and tribological behaviors over unreinforced polymers [1]. Among the different kinds of PMCs, polytetrafluoroethylene (PTFE) matrix composites show more improved mechanical and tribological behaviors than neat PTFE matrix. They are used as tribological components in some sectors as a result of their high strength and better tribological behaviors [2]. PMCs have indicated important enhancements in tribological behaviors, such as abrasive and sliding wear resistance [3]. Therefore, more attention has been channeled towards reinforcing polymer matrices for tribological applications in

lightweight, load bearing, and tribological conditions. For tribological applications, it has been shown that if PMCs are potential candidates in abrasive conditions [4,5]. For PTFE matrix composites, it is generally agreed that increasing the fibre content might improve or weaken its tribological behaviors [6,7]. PMCs with better tribological behaviors are used as brakes and clutches in automobiles and aircrafts [8,9]. PTFE continues to receive attention in tribological conditions for its low coefficient of friction, ease of processability, chemical inertness, low density, and low cost [10,11].

A frequent problem that occurs in industries is abrasive tribology. Many authors have experimentally studied the abrasion of polymer matrices and PMCs. For example, Kunigal and Kumar [4] added nano-clay and discontinuous carbon fibre to a PA66/PP matrix. Different behaviors were observed on the addition of the reinforcements. Nano-clay-reinforced PA66/PP composite indicated better abrasion compared to carbon-reinforced PA66/PP composite [4]. Shipway and Ngao [12] studied the abrasion behaviors of different polymers and found that the polymers exhibited different abrasion behaviors. Moreover, it was revealed that distance was the most significant parameter influencing the abrasion behavior [12]. Suresha, Ravi, Suresha, and Venkataramareddy [13] investigated the abrasive wear of vinyl/ester matrices reinforced with glass and carbon fabric reinforcements. The results showed that vinyl/ester strengthened with carbon fabric demonstrated a lower tribological rate than glass-reinforced vinyl/ester composite [13]. As reported by Liu et al., in particles filled with ultra-high molecular weight polyethylene (UHMWPE) matrix composites, the improvement of the abrasion property was attributed to the particles' stiffness; in terms of the experimental parameter, it was found that applied load was the most significant parameter [14]. In their study of the coefficient of the friction and abrasion behavior of epoxy reinforced with betelnut filler, Yousif, Nirmal, and Wong [15] found that sliding the composites against coarser grains led to the maximum tribological rate. Similarly, mass loss increased when sliding velocity maximum [15].

The above illustrates experimental studies that seem to be tedious and cumbersome. Thus, the design of experiment (DOE), a statistical tool that minimizes and simplifies experiments, thereby saving cost, time, and energy [16], was introduced. A commonly used DOE method is the Taguchi orthogonal array (OA). It is an efficient, simple, and cheap method of optimization. It has been widely applied in the optimization of the tribological behaviors of PMCs, as will be illustrated in the following sections. Sudarash, Varadarajan, and Rajendra optimized the tribological parameters of PMCs, and the results showed that applied load was the most influential factor affecting the wear rate [17]. Ramesh and Suresha arranged the significance of factors influencing the abrasion behaviors of reinforced carbon epoxy composites as filler content > grit size > filler type [18]. Similar findings were obtained in the study of graphite and silicon carbide reinforced composites under dry conditions [19]. Cho Pogosian and Bahadur reported that particle content was the most influential factor influencing the tribological rate of polyphenylene sulfide matrix composites [20]. Chauhan and Thakur (2013) optimized the friction and sliding wear of submicron size cenosphere particle-reinforced vinyl ester composites [21]. Cenosphere filler was the most influential parameter on coefficient of friction and wear rate, as seen in the analysis of variance (ANOVA) results [21]. In his study of PTFE-filled composites, Şahin established that grit size was the most significant parameter, followed by load, distance, and flexural strain [22]. Sudarshan looked into the influence of filler content, load, and distance on the abrasive wear property of epoxy-reinforced matrix composite. According to the findings, it was demonstrated that sliding distance was the most influential factor affecting the wear rate [23]. Darshan, Suresha, and Jamadar [24] studied the effect of parametric wear rate of Hallosyte nanotube reinforced basalt/silk epoxy composite. Four parameters viz abrading distance, amount of filler, applied load, as well as silica sand size at three levels were considered. The results showed that abrading distance was the most influential control factor that affected the wear rate [24]. The Taguchi method establishes single parameter significance. Consequently, to establish multiple significance, the Taguchi method has been coupled with grey relational analysis (GRA). Dharmalingam, Subramanian, and

Kok [25] combined the Taguchi approach with GRA to optimize the abrasive tribological property of aluminum hybrid metal composites. It was found that grit size and applied load were the most significant parameters affecting the wear rate and coefficient of friction, respectively, of the composites [25]. Based on the mean response Taguchi–GRA results, Sylajakumar, Ramakrishnasamy, and Palaniappan [26] found that load at 60 N, a speed of 1 ms^{-1} , and a distance of 1000 m were the optimal control factors. ANOVA revealed that distance gave the highest contribution of 61.05% to the wear rate of the C4 composites. An improvement of 35% in the grey relational grade was achieved on validation [26]. Savaran and Thanigaivelan [27] used the same approach hybridized with principal component analysis (PCA) for the optimization of the laser parameters of the dimple geometry of stainless steel. It was found that that optimal GRG peak value of 0.2642 was obtained at an average power of 12 W, pulse duration of 1500 ns, and a frequency of 15 Hz. ANOVA showed that average power was the most significant parameter, while depth was of little or no importance [27].

The prediction of the abrasive tribological behaviors of PMCs is not an inconsequential role, and the departure from generality behaviors are common. Generally, it is difficult to predict the tribological behaviors of PMCs due to the interdependencies among the process variables. Tribological modelling usually entails a significant number of experiments together with analytical modeling and/or numerical simulation, leading to high costs, time consumption, and energy losses. As a panacea to this, the use of machine learning to build predictive models that can function with relatively small datasets and are capable of drawing conclusions regarding nonlinear, complex, and noisy data is essential. Different artificial intelligence (AI) models, such as artificial neural networks (ANN), adaptive neuro-fuzzy inference systems (ANFIS), and support vector regression (SVR) models, have been applied in different aspects of tribology. Velten, Reinicke, and Friedrich [28] employed ANN to predict the wear rate of a PTFE matrix strengthened with discontinuous carbon and glass fibre composites. The prediction accuracy of the models was also influenced by the amount of training. The ANN results showed better agreement with the trial results [28]. ANNs were also used by Zhang, Friedrich, and Velten [29] to predict the volume loss and coefficient of friction of glass-reinforced polyamide matrix composites. To search for the optimal model, five different learning algorithms were tried. The learning algorithm results showed that the Levenberg–Marquardt algorithm was the optimum, having a prediction capacity of 87.59%. The predicted outputs showed reasonable agreement with the measured outputs [29]. Equally, ANNs were used to predict the tribological and mechanical properties of behaviors and the mechanical properties of short-fibre PMCs [30,31]. The prediction performance of the ANN model was compared with the ANFIS model by Haghigat, Semnani, and Nouri in the specific wear loss prediction of graphite-, carbon-, and nano-TiO₂-filled PTFE matrix composites. After trying different learning algorithms for ANN, the LM algorithm was the best, while for the ANFIS model, the trapezoidal membership function was the best. The comparative results showed superior prediction performance to the ANN model [32]. Taguchi–ANN has been used to optimize and predict the abrasion of industrial waste and glass-filled polyester matrix composites. The combination of optimal parameters for minimum wear was found to be 1.8 ms^{-1} –10 N–15 %–80 m for industrial waste, and for glass-reinforced polyester matrix composite, the combination was 2.10 ms^{-1} –10 N–15 %–70 m for the speed, load, filler amount, and distance, respectively. The ANN predictions showed better performance than the linear regression model [33]. The SVR model was used in the prediction of the tool flank wear performance of machine surface [34], the tool wear face milling of mild steel [35], and the diameter of PCL/gelatin [36]. The ANN model was compared with the Harris Hawk optimization (HHO) model in the optimized prediction of the abrasive tribological behavior of ultra-high-strength martensitic steel. The prediction results of the models revealed that the ANN–HHO model gave better prediction than the ANN as a single model [37].

Although AI models indicate practical and promising capabilities in the field of material sciences, they are still associated with certain limitations and challenges such as numerous and qualitative data, which serve as the prerequisite requirements. Even though various material characteristic databases are accessible, discrepancies in the data provided by different parties make machine learning algorithms difficult to apply effectively. Machine learning models are also known to break the principles of physical science, because they are frequently driven solely by the data provided and do not take into account any chemistry/physics-based knowledge. A survey of the reported literature on the database Scopus yielded the finding that there were 450 peer-reviewed papers, from 1989 to date, focusing on the abrasive tribological behaviors of PTFE matrix composites, indicating the wide range of interest in this topic. Figure 1b shows 388 keywords that occurred among those studies, indicating the deep interest and implementation in this field. In addition, the popularity of this study topic was investigated in different regions throughout the world, with the bulk of the countries producing output being China, the United States, and India (Figure 1a). The motivation of this study demonstrated excellent AI models for the prediction of the abrasive tribological behaviors of PTFE matrix composites. Generally, each study progressed to a higher degree of accuracy for observations and efficiency at a deeper level than the previous one. To the best knowledge of the authors, no study published in technical literature has predicted the abrasive tribological behaviors of PTFE matrix composites employing this approach. As a result, the goal of this work is to perform multi-response optimization and to predict the abrasive tribological behaviors of PTFE matrix composites using hybridized Taguchi and novel AI hybridized SVR models, respectively.

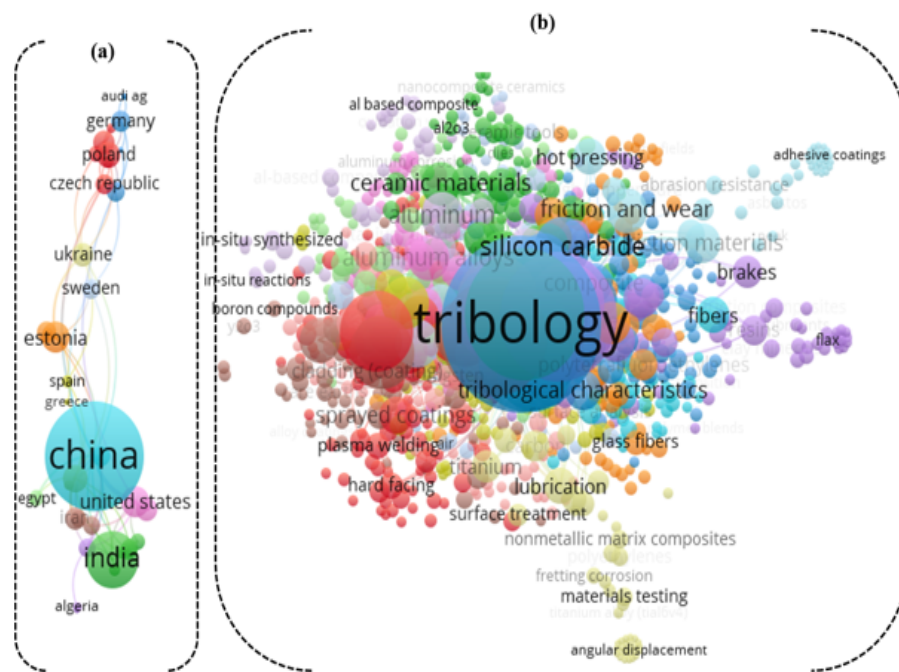


Figure 1. (a) Major keywords used in the literature on the abrasive tribology of PTFE-based composites (1989–2021); (b) the investigated research areas for abrasive tribology.

2. Materials and Methods

2.1. Materials

The materials used in this article are the PTFE matrix, and carbon- and bronze-filled PTFE composites. Produced using the compression molding process, the materials in rectangular forms were supplied by Polymer Chemical Industry Ltd., (Gebze, Turkey). At present, these materials are used in the automotive and aerospace industries. The materials, their codes, and some selected properties are shown in Table 1. Computer numerical water jet machining was used to cut samples for the tests from the rectangular plaques,

whose dimensions were 500 mm × 500 mm × 6 mm. Thereafter, the samples were cleaned before the experiments. Silicon carbide (SiC) particles of sizes in the range of 150, 400, and 1000 meshes were used as abrasives.

Table 1. Physical and mechanical properties of materials used in the study.

Samples	Code	ρ (gcm^{-3})	σ (Kgcm^{-2})	ϵ at Break (%)
Bronze–PTFE composite	BF40	3.15	280	280
Carbon–PTFE composite	CF25	2.15	210	110
Polytetrafluoroethylene	PTFE	2.1	380	400

2.2. Method

2.2.1. Test Conditions

The abrasive tribological testing conditions were developed based on the design of experiment (DOE) technique. DOE is an optimization method to find the optimal process parameter. In this study, four parameters, namely, load (L, N), grit size (G, mesh), sliding distance (SD, m), and sliding speed (SS, ms^{-1}), at three levels were treated for the configuration of the experimental trials (Table 2). Twenty-seven trials were performed based on the Taguchi L_{27} (3^4) orthogonal array (OA). The results of the Taguchi L_{27} (3^4) OA obtained from Minitab 2019 are provided in Table 3. Four responses, namely, mass loss (M_L , g), volume loss (V_L , mm^3), coefficient of friction (μ), and specific tribological rate (K_s , $\text{mm}^3\text{N}^{-1}\text{m}^{-1}$) were optimized. The signal-to-noise-ratios (the smaller the better) logarithmic function, coded as SNRs_{STB} , was used to determine the optimal process parameters (Equation (1)). The SNRs_{STB} for the responses was computed using Equation (1) for the 27 trials. The results are provided in Table 3. The highest SNRs give the desired response.

$$(\text{SNRs})_{\text{STB}} = - \log 10 \frac{1}{n} (\sum_{i=0}^n (y_i)^2) \quad (1)$$

where n = number of experiments and y_i = experimental value.

Table 2. Control factors and their levels.

Symbol	Control Factors	Level 1	Level 2	Level 3
L	Load, (N)	3	6	9
G	Grit size, (mesh)	1000	400	150
SD	Sliding distance, (m)	25	45	55
SS	Sliding speed, (ms^{-1})	0.04	0.08	0.14

2.2.2. Abrasive Wear Test Method

An abrasive wear test of the PTFE matrix composites was conducted using an Arton Paar tribometer (made in Switzerland), as shown in Figure 2 according to the ASTM G99 standard. SiC papers were placed on a mild steel disk by means of glue and fixed to the spindle of the tribometer. The samples were then inserted into a specially designed fixture. Afterwards, the fixture, together with the sample, was fixed to a steel holder in the tribometer normal to the flat surface of the rotating counter mild steel disk. During this work, all samples were tested as per the matrix design in Figure 3 and Table 3, and contrived using the DOE technique. The design matrix encompasses the various combinations of the input parameters used to perform the test. The mass loss was measured using PS 1000.RS RADWAG digital weighing machine (made in Poland) with 10^{-3} g sensitiveness, and was mathematically computed using Equation (2).

$$M_L = m_b - m_a \quad (2)$$

The volume loss was computed using Equation (3):

$$V_L = \frac{M_L}{\rho} \quad (3)$$

μ was computed and displayed by the computer attached to the tribometer. K_s was obtained by converting mass loss into volume loss using density data via Equation (4):

$$K_s = \frac{M_L}{\rho L D} \quad (4)$$

where M_L = mass loss (g), V_L = volume loss (mm^3), m_b = mass before test (g), m_a = mass after test (g), ρ = (gcm^{-3}), L = load in N and D = sliding distance (m). Each trial was performed twice and averaged.

Table 3. Signal noise ratio of against SiC particle based on Taguchi L₂₇(3⁴) OA.

Trial	L (N)	G (mesh)	SD (m)	SS (ms^{-1})	M_L SNR (dB)	V_L SNR (dB)	μ SNR (dB)	T_S (dB)
1	1	1	1	1	57.39	63.84	19.05	101.34
2	1	1	1	1	53.76	60.00	12.09	97.50
3	1	1	1	1	52.96	62.64	15.42	100.14
4	1	2	2	2	46.20	52.64	14.29	95.25
5	1	2	2	2	44.08	50.32	11.09	92.92
6	1	2	2	2	50.90	60.59	10.86	103.20
7	1	3	3	3	47.64	54.08	17.49	98.43
8	1	3	3	3	44.58	50.82	12.90	95.17
9	1	3	3	3	40.72	50.41	5.47	94.76
10	2	1	2	3	51.54	57.98	11.26	106.61
11	2	1	2	3	61.41	67.65	13.87	116.27
12	2	1	2	3	50.03	59.72	13.07	108.35
13	2	2	3	1	52.40	58.84	10.36	109.21
14	2	2	3	1	46.84	53.07	17.96	103.45
15	2	2	3	1	44.08	53.77	0.36	104.14
16	2	3	1	2	43.48	49.92	19.05	93.44
17	2	3	1	2	41.21	47.44	5.09	90.97
18	2	3	1	2	40.96	50.65	6.98	94.17
19	3	1	3	2	50.31	56.76	8.68	110.65
20	3	1	3	2	50.60	56.84	29.50	110.73
21	3	1	3	2	50.03	59.72	26.20	113.61
22	3	2	1	3	46.94	53.38	21.36	100.42
23	3	2	1	3	44.66	50.89	18.75	97.94
24	3	2	1	3	44.81	54.49	11.04	101.54
25	3	3	2	1	45.76	52.21	7.90	104.36
26	3	3	2	1	40.31	46.54	10.80	98.69
27	3	3	2	1	37.82	47.51	10.24	99.66



Figure 2. Arton Paar tribometer used for the experiment.

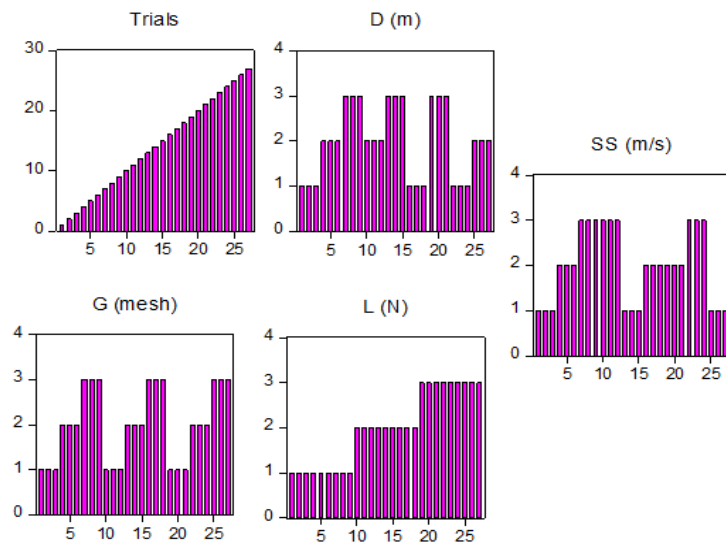


Figure 3. Taguchi $L_{27}(3^4)$ OA.

2.3. Multi-Response Optimization through Grey Relational Analysis (GRA)

The Taguchi approach is only capable of optimizing a single response. However, when two or more responses of distinct features are involved, the Taguchi technique is limited. Thus, an optimization method called grey relational analysis (GRA) becomes a panacea. Taguchi OA was used to obtain the optimal levels of the tribological parameters. Data normalization is categorized as “the smaller the better” and “the larger the better”. Let the actual sequence and the comparison sequences be $X_i^*(k)$ and $\varphi_i(k)$, respectively. $i = 1, 2, 3 \dots ; m = 1, 2, 3 \dots$ and n and m represent the total number of experiments and experimental values, respectively. Data preprocessing is used to transform the actual sequence into an identical sequence. Many data preprocessing techniques can be utilized in GRA, depending upon the features of the actual sequence. Generally, the series is normalized between 0 and 1 [27].

For this study, the target value is “the smaller the better”. Therefore, the actual sequence is normalized using Equation (5):

$$X_i^*(k) = \frac{\max\varphi_i(k) - \varphi_i(k)}{\max\varphi_i(k) - \min\varphi_i(k)} \quad (5)$$

where $X_i^*(k)$ = normalized for the i th experiment and $\varphi_i(k)$ = initial sequence of the average responses.

After data normalization, the succeeding phase is the computation of the deviation sequence of the normalized data using the mathematical Equation (6), shown below:

$$\Delta_{oi}(k) = |X_0^*(k) - X_i^*(k)| \quad (6)$$

where $\Delta_{oi}(k)$ stands for deviation, $X_0^*(k)$ denotes the normalized data, and $X_i^*(k)$ refers to the comparability sequence. GRC is thus estimated through Equation (7):

$$\xi_i(k) = \frac{\Delta_{min} + \zeta\Delta_{max}}{\Delta_{oi}(k) + \zeta\Delta_{max}} \quad (7)$$

where $\xi_i(k)$ = GRC of each response, Δ_{min} and Δ_{max} = the lowest and the highest deviations of the individual target factor, respectively. The differentiating or identification coefficient is symbolized by ζ and is demarcated within the range of $\zeta \in [0, 1]$. This is usually set at $1/2$.

to assign equivalent weights to every variable. As indicated in Equation (8), the GRG is then determined by taking the mean of the GRG of each output parameter:

$$\gamma_i = \frac{1}{n} \sum_{i=1}^n \xi_i(k) \quad (8)$$

where γ_i = GRG obtained for i th test run, and n = summation count of performance attributes. Following the determination of the optimal levels of the parameter, the last phase is to predict and validate the result using Equation (9):

$$\gamma_{predicted} = \gamma_m + \sum_{i=1}^q \gamma_0 - \gamma_m \quad (9)$$

where γ_0 represents the highest of the mean GRG at optimum levels of the variables and γ_m defines the average GRG. q = parameter that signifies the factors influencing the target values.

To find out the contribution of each parameter on the wear rate, an ANOVA is applied. A large percentage contribution (%C) signifies a parameter exerting a significant influence on the responses.

2.4. Artificial Intelligence Techniques

2.4.1. Support Vector Regression (SVR)

In 1995, Vapnik put into practice a support vector machine (SVM): an observed-based learning approach. The minimization of structural risk as well as statistical learning theory are the most important functions of the SVM. Nevertheless, the properties that distinguish SVM from ANN are complexities, minimization in error, and gain in the network's performance capability. SVM can be categorized into linear support regression and nonlinear support regression (NSVR). SVR can be considered an SVM on the basis of layers that entail the kernel function's weight on the input data as well as the function sum of the weighted kernel function of the data targets. By and large, SVM is codified to two codes, namely, support vector regression (SVR) and support vector classifier (SVC). SVR deals with prediction, whereas SVC treats classification problems. SVR is designated as:

$$f(x) = w \times \Phi(x) + b \quad (10)$$

where w = vector's weight displayed in the feature space, Φ = transfer function, and b = bias. Therefore, problems involving SVR function $f(x)$ are given as:

$$\text{Minimize : } \frac{\|w\|^2}{2} + C \left[\sum_{i=1}^N \xi_i + \xi^* \right] \quad (11)$$

subject to the conditions:

$$y_i - f(x) \leq +\varepsilon + \xi_i \quad (12)$$

$$f(x) - y_i \leq +\varepsilon + \xi^* \quad (13)$$

$$\xi_i, \xi^* \geq 0, i = 1, 2, \dots, N \quad (14)$$

where $\|w\|^2$ = weight norm vector, C = penalty parameter, ξ_i and ξ^* = slack variables. By using Lagrange functions, the solution of the non-linear regression function is presented according to the optimization:

$$f(x) = \sum_{i=1}^N (\alpha_i - \alpha_i^*) K(x, x_i) + b \quad (15)$$

where $K(x, x_i)$ = kernel function and $(\alpha_i \text{ and } \alpha_i^* > 0)$ = binary variables. There exist several kernel functions, including sigmoid, linear, and polynomial, but the most commonly used

kernel function is the radial basis function (RBF). Consequently, the RBF kernel was used in this article. The RBF kernel adopted here is provided below.

$$K(x, x_i) = \exp(-\gamma \|x_i - x\|^2) \quad (16)$$

where γ = kernel parameter. SVR performance is affected by three parameters, which are C , γ , and ϵ (size).

2.4.2. Harris Hawk Optimization (HHO)

HHO is a unique algorithm calculated by simulating the hawk's hunting process. Recently, the procedure has been used with success in solving several intricate engineering and science issues. The hawks mostly operate alone, whereas the Harris hawks pursue and hunt in groups. Hence, the HHO method typifies the cooperation method and hunting characteristic of the natural Harris hawks. The hunting entails tracing, encircling, approaching, and attacking, and is achieved in three main phases: exploration, a transition from exploration to exploitation, and exploitation (Figure 4).

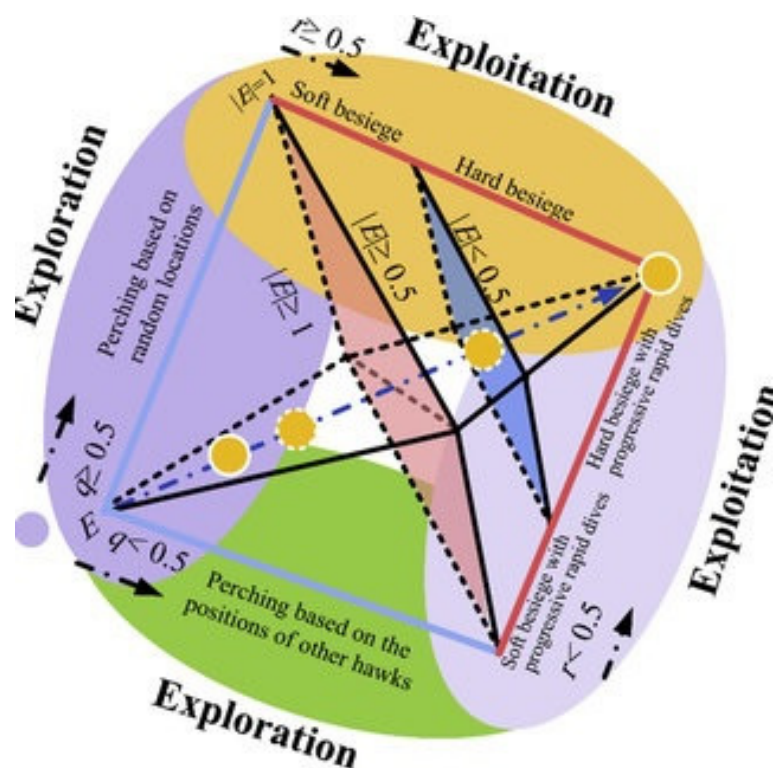


Figure 4. Various phases involved in HHO [38].

2.4.3. Particle Swarm Optimization (PSO)

In 1995, the scientists Kennedy and Eberhart presented the SPO algorithm. An algorithm inspired by the social feature and dynamics of animals, SPO is population-based. Its first purpose was to clearly mimic animals' social behavior, for example bird flocking, to detect the trends that control the capability of birds to fly at precisely the same time and to all of a sudden change direction while regrouping in optimum formation. Since this first purpose, the idea transformed into an efficient and simple optimization technique. PSO is initialized with a group of random particles that look into an optimum value by updating the two best values in each repetition. The first is named the personal best, or pbest, which is the best value obtained so far by any particle within the population. All of the particles explore the search space and the information collected by them is utilized for

finding the best particle in the swarm, referred to as global best, or gbest. Thereafter, the particle updates its velocity and positions according to Equations (14) and (15):

$$V_i^{k+1} = \omega V_i^k + c_1 r_1 \times (pbest_i^k - X_i^k) + c_2 r_2 \times (gbest^k - X_i^k) \quad (17)$$

$$X_i^{k+1} = X_i^k + V_i^{k+1} \quad (18)$$

where V_i^{k+1} = the velocity of individual I at iteration $k + 1$, V_i^k = the velocity of individual i at iteration k , ω stands for inertia weight parameter, c_1 and c_2 show the cognitive parameters, r_1 and r_2 = random numbers between 0 and 1, X_i^k = position of individual i at iteration k , $pbest_i^k$ = the best position of individual I at iteration k , and $gbest^k$ indicates the best position of the group until iteration k . Figure 5 shows the flowchart of the PSO algorithm.

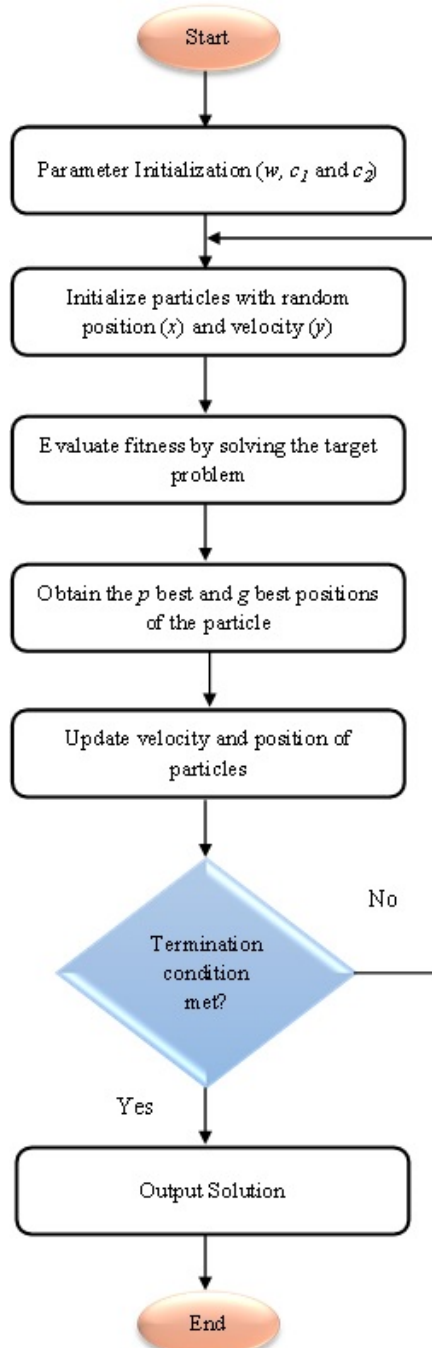


Figure 5. PSO algorithm flow chart [39].

2.4.4. Hybrid SVR Algorithm

Improving the performance of the single SVR model needs a cautious delineation of the SVR model's parameters. The robustness of the SVR model relies upon the precise choice of the parameters. Yet, when there is a wider range of parameters, the search space becomes larger, thereby making the choice of precise parameters hard. Therefore, this issue can be addressed as an optimization issue, and needs to be resolved via optimization methods. The integration of the SVR model with PSO as well as HHO algorithms inspired by nature gave birth to the SVR-PSO and SVR-HHO hybrid models. The nature-inspired algorithms were utilized to choose the SVR model's parameters. Flow chart of the proposed hybrid models is shown in Figure 6.

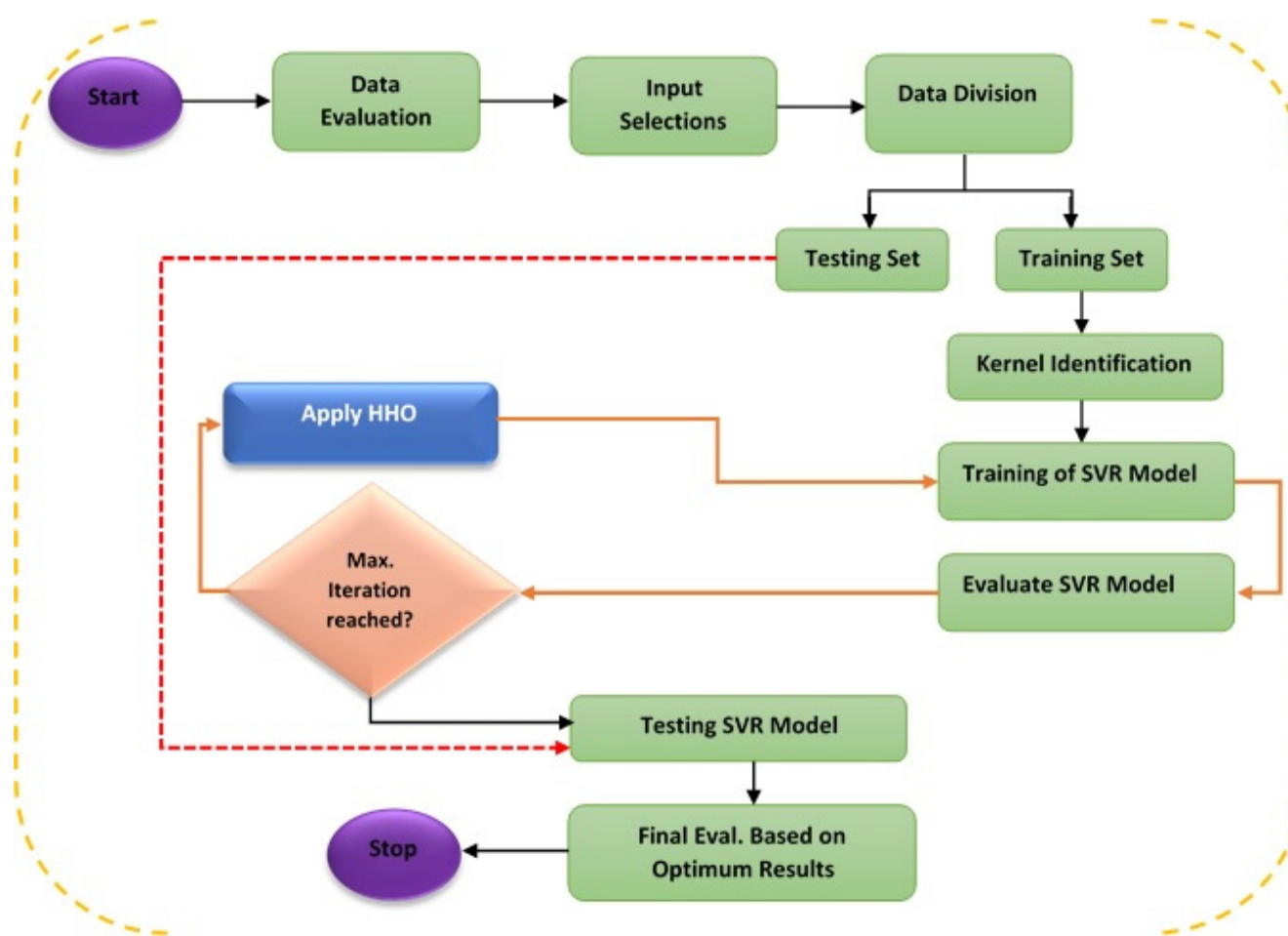


Figure 6. Flow chart for the proposed hybrid models [39].

2.5. Data Pre-Processing, Model Validation, and Performances Metrics

One of the significant aims of any AI model is to ascertain that the model conforms to acceptable data based on the model's evaluation metrics utilized to obtain a dependable and strong computed outcome of the unknown data. Nevertheless, overfitting and local minima problems occur in the data validation. Hence, the performance of the learning phase might be unsatisfactory. This is especially true when the analysis deals with a relatively small dataset, as in this study. Various validation methods can be employed, including cross-validation (k -fold), hide-out, and leave one out. Here, the k -fold approach was used to repeal overfitting issues. With respect to this study, the data were split into 70% and 30% for calibration and validation, respectively. The results of the tribological experiments were pre-processed and normalized according to Equation (16). Data normalization was performed prior to model training. Data normalization enhances the prediction accuracies of the models. The current work introduced the SVR model coupled with PSO and HHO models

to predict the abrasive tribological behaviors of PTFE matrix composites. The prediction of tribological behaviors is important. However, the creation of a reliable model is often challenging and difficult given the nature of the dataset obtained from the experiments.

Normalized data:

$$y = \left(\frac{x - x_{min}}{x_{max} - x_{min}} \right) \quad (19)$$

where y = normalized data, x = is the experimental data, and x_{max} and x_{min} are the maximum and minimum experimental data, respectively.

For the purpose of appraising the prediction accuracies of the models, the frequently used evaluation metrics of determination coefficient (R^2), correlation coefficient (R), mean square error (MSE), root mean square error (RMSE), and mean absolute percentage error (MAPE) were used. These are mathematically given in the equations below.

$$R^2 = 1 - \frac{\sum_{i=1}^N (x - y)^2}{\sum_{i=1}^N (x - \hat{x})^2} \quad (20)$$

$$R = \frac{\sum_{i=1}^N (x - \hat{x})(y - \hat{y})}{\sqrt{\sum_{i=1}^N (x - \hat{x})^2 \sum_{i=1}^N (y - \hat{y})^2}} \quad (21)$$

$$MSE = \frac{1}{N} \sum_{i=1}^N (x - y)^2 \quad (22)$$

$$RMSE = \sqrt{\frac{\sum_{i=1}^N (x - y)^2}{N}} \quad (23)$$

$$MAPE = \frac{1}{N} \left[\sum_{i=1}^N \left| \frac{x - y}{x} \right| \right] \quad (24)$$

where x , y , \hat{x} and \hat{y} = actual, predicted, average actual, and average predicted values, respectively.

3. Results and Discussion

3.1. Results for Mass Loss, Volume Loss and μ

Figures 7 and 8 show mass and volume losses as a function of load, grit size, sliding speed, and sliding distance. From Figures 8 and 9, it can be seen that increasing the load increased the mass and volume losses, but decreased when the sliding distance and sliding speed increased. Maximum mass and volume loss were obtained at 9 N, 150 mesh, 45 m, and 0.08 ms^{-1} , while minimum mass and volume losses occurred at 3 N, 1000 mesh, 55 m, and 0.14 ms^{-1} . This observable fact indicates that different wear mechanisms are perhaps involved. At higher loads, the abrasive particles penetrate deeply into the materials, causing ploughing and separation of the fibres from the matrix.

3.2. Abrasive Tribological Rate (T_s) and Coefficient of Friction (μ)

Figures 9 and 10 display the graphs of μ and T_s versus load, grit size, sliding distance, and sliding speed. From Figure 9, it can be deciphered that μ was low at 3 N, and then suddenly increased and decreased at 6 N and 9 N, respectively. Moreover, increasing the sliding distance increased the μ , but it decreased with a corresponding increase in grit size and sliding speed. From Figure 10, it is evident that increasing the load, grit size, sliding distance, and sliding speed led to a decrease in the abrasive wear rate of the PTFE matrix composites. As presented in Figure 10, T_s decreased with an increase in load, sliding distance, sliding speed, and grit size. Initially, T_s was high for load, grit size, and sliding distance, but high at the second level for sliding speed. The abrasive wear rate decreased sharply when tested against 400 mesh (i.e., from 150–400 mesh). Moreover, a linear decreasing trend was noticed with an increase in the load from 3 to 6 N and a sliding

distance from 25 to 55 m. However, it increased slightly with an increase in speed and decreased suddenly at high sliding speeds.

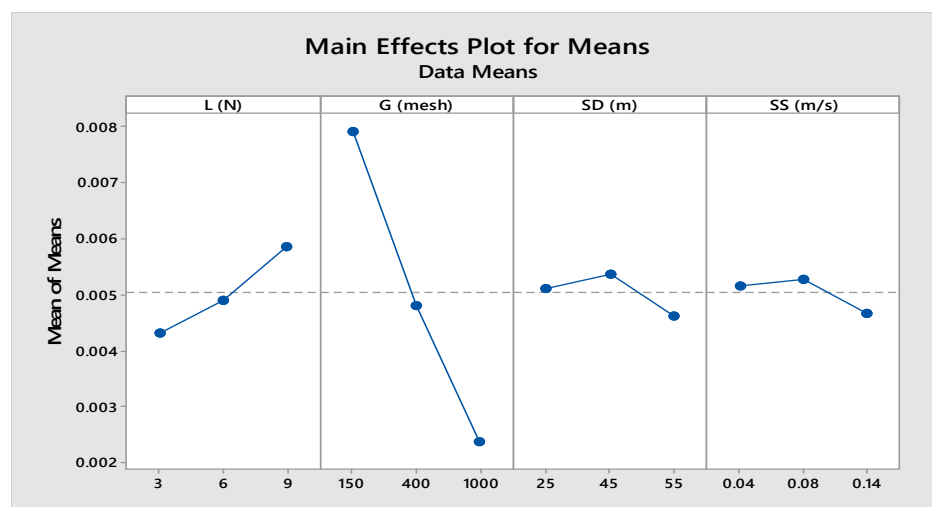


Figure 7. Main effect plot for mean mass loss of PTFE matrix composites.

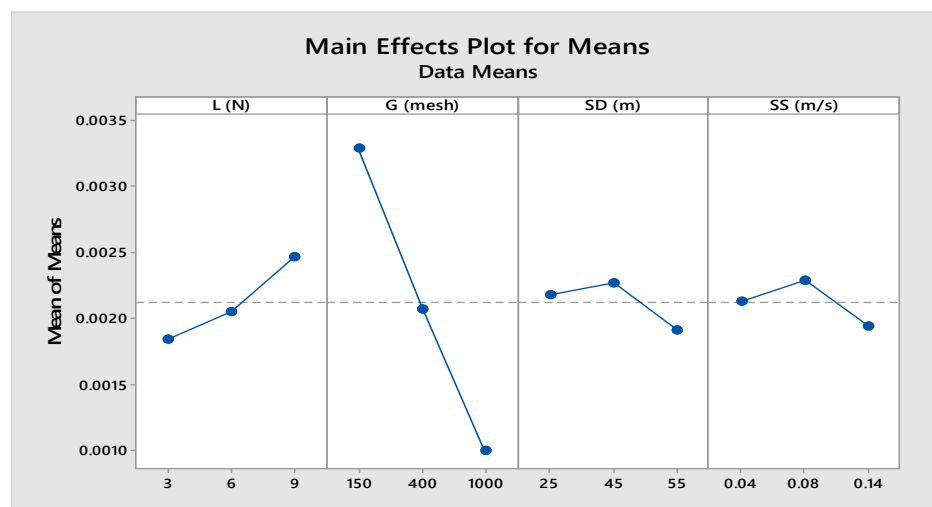


Figure 8. Main effect plot for mean volume loss of PTFE matrix composites.

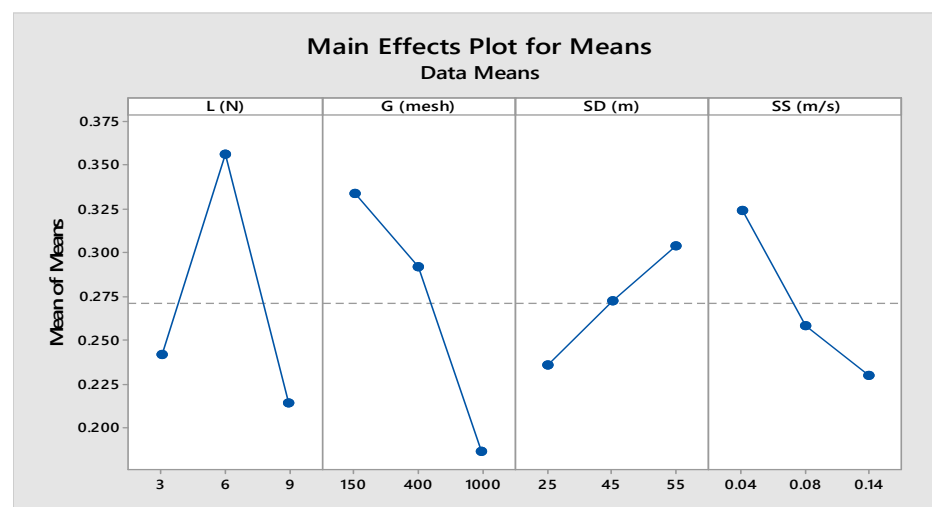


Figure 9. Main effect plot for mean μ of PTFE matrix composites.

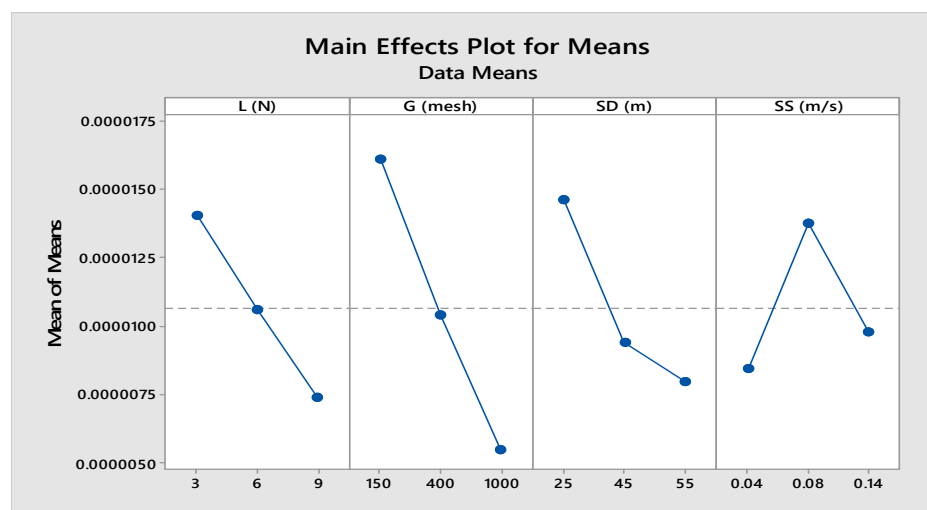


Figure 10. Main effect plot for mean T_s of PTFE matrix composites.

3.3. Single Response Optimization and ANOVA

The computed SNRs response table for M_L , V_L , μ , and T_s are shown in Tables 4–7, respectively. The maximum value of SNRs at the main effect plot for SNRs gave the desired results. Bolded values in the response tables for SNRs show the desired SNRs.

Table 4. Response table for SNRs of M_L (smaller is better).

Level	L (N)	G (mesh)	SD (m)	SS (ms^{-1})
1	47.99	41.80	47.14	47.05
2	46.88	46.07	46.26	46.10
3	45.30	52.31	46.78	47.02
Delta	2.70	10.52	0.88	0.95
Rank	2	1	4	3

Table 5. Response table for SNRs of V_L (smaller is better).

Level	L (N)	G (mesh)	SD (m)	SS (ms^{-1})
1	55.39	49.58	54.54	54.86
2	54.65	53.36	53.75	53.17
3	52.65	59.89	54.55	54.80
Delta	2.60	10.31	0.80	1.69
Rank	2	1	4	3

Table 6. Response table for SNRs of μ (smaller is better).

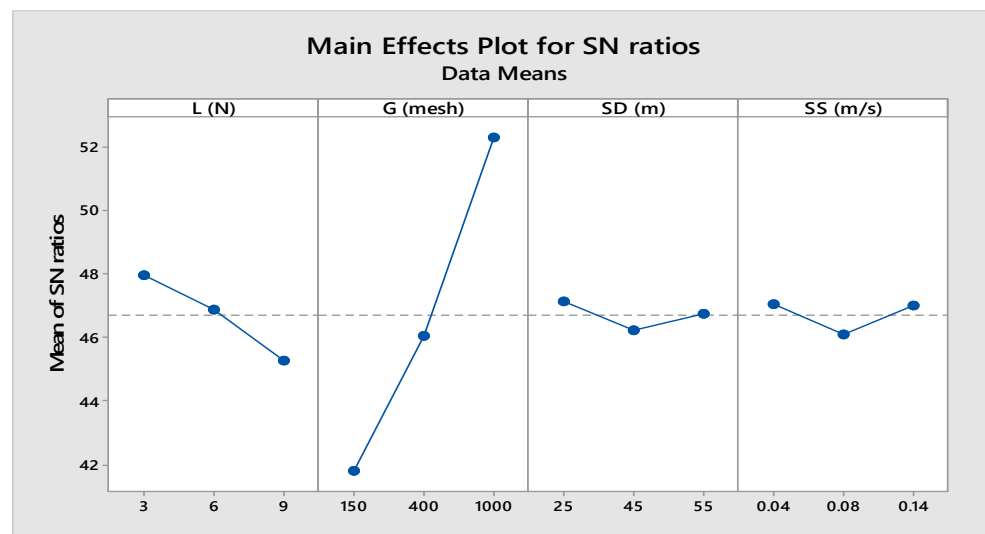
Level	L (N)	G (mesh)	SD (m)	SS (ms^{-1})
1	11.92	8.78	12.35	9.59
2	8.28	10.42	11.29	10.92
3	12.53	13.53	9.09	12.3
Delta	4.27	4.75	3.25	2.64
Rank	2	1	3	4

Table 7. Response table for SNRs of T_s (smaller is better).

Level	L (N)	G (mesh)	SD (m)	SS (ms^{-1})
1	96.88	96.26	97.23	101.54
2	102.16	100.03	101.54	99.85
3	103.82	106.57	104.09	101.47
Delta	6.94	10.31	6.86	1.69
Rank	2	1	3	4

Based on Table 4 and Figure 11, the optimum process variables for obtaining low M_L using the Taguchi technique were found to be $L = 3 \text{ N}$, $G = 1000 \text{ mesh}$, $SD = 25 \text{ m}$, and $SS = 0.04 \text{ ms}^{-1}$. The corresponding level values are presented in bold to facilitate understanding of the mean SNRs response table. This predicted combination of optimum parameters for M_L was coded as L1G1SD1SS1. According to Table 5 and Figure 12, the estimated optimum settings for achieving minimum V_L was determined to be $L = 3 \text{ N}$, $G = 1000 \text{ mesh}$, $SD = 55 \text{ m}$, and $SS = 0.04 \text{ ms}^{-1}$. This combination of optimum settings is coded as L1G3SD3SS1. From Figure 13 and Table 6, it was observed that the maximum mean SNRs achieved for μ were L at 9 N, G at 1000 mesh, and SD at 25 m, and SS at 0.14 ms^{-1} . Thus, the estimated optimum process parameter settings for achieving a minimum μ via the Taguchi method can be coded as L3G1SD1SS3. As seen in Figure 14 and Table 7, the highest mean SNRs obtained for T_s were L at 9 N, G at 1000 mesh, and SD at 55 m, and SS at 0.04 ms^{-1} . Therefore, using the Taguchi method, the predicted optimum parameter settings are styled as L3G1SD3SS1.

ANOVA depicts the parameters that significantly influence the abrasive behaviors. The ANOVA for M_L showed that G was the most significant parameter, followed by L , SD , and SS as 97.26%, 1.12%, 0.96%, and 0.65%, respectively. With regard to the V_L , the ANOVA indicated that G with 90.29% was the most influential parameter affecting the V_L , followed by L (5.96%), SS (3.04%), and SD (0.71%). The analysis for μ found G as the most significant parameter, having a percentage contribution of 37.24%, followed by L with 33.92%, SD with 17.62%, and SS with 11.20%. Equally, G was found to be the most influential parameter contributing to minimum T_s , showing 65.00%, while L showed 65%, SD 22.57%, and SS 1.72%

**Figure 11.** Main effect plot for SNRs of mean M_L .

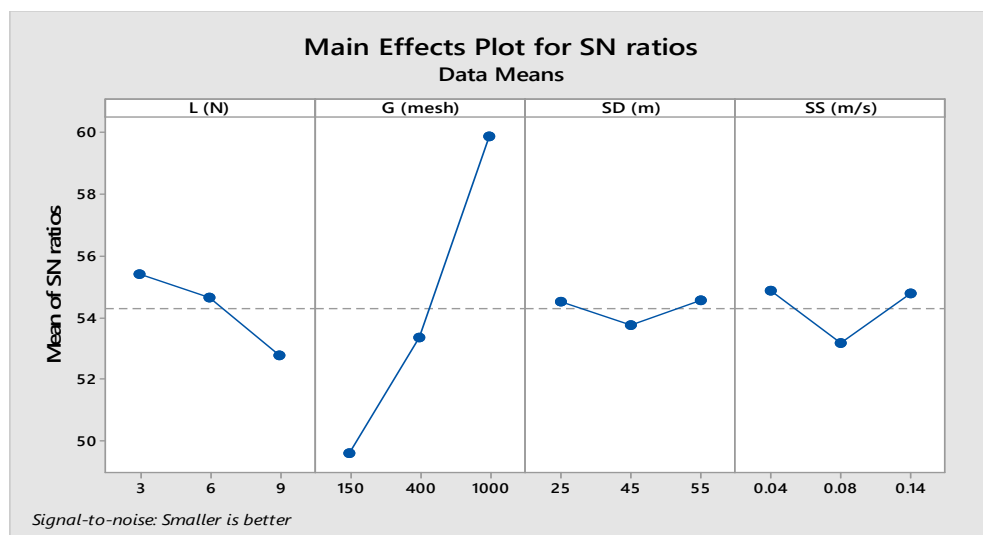


Figure 12. Main effect plot for SNRs of V_L .

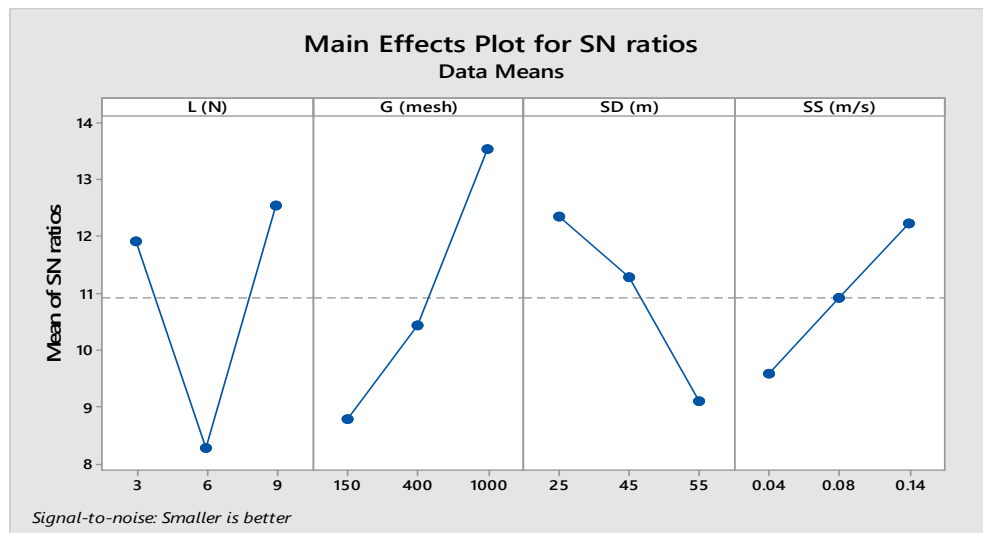


Figure 13. Main effect plot for SNRs of mean μ .

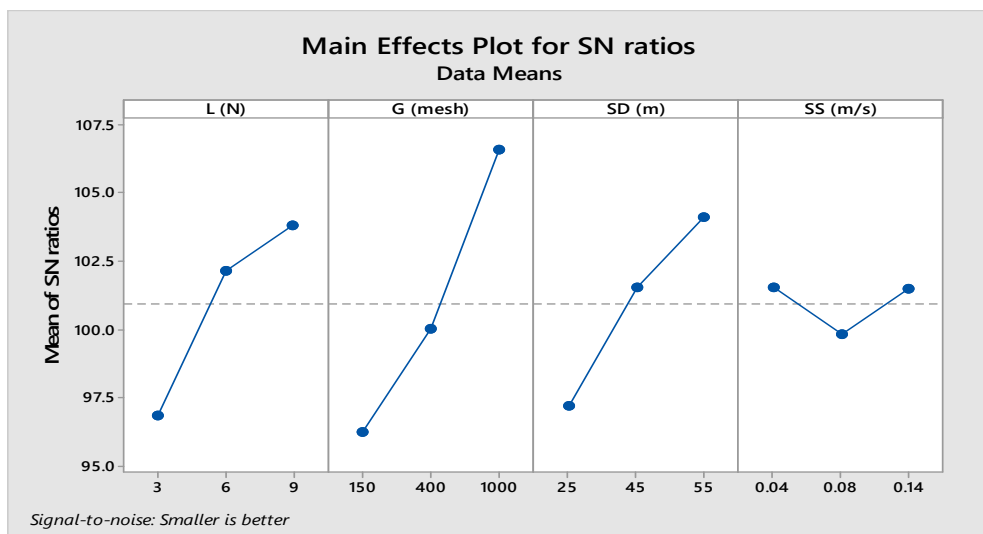


Figure 14. Main effect plot for SNRs of T_s .

3.4. Multi-Response Optimization Using Grey Relation Analysis Optimization Using GRA and ANOVA

As seen above, the Taguchi technique is only capable of optimizing a single parameter at a time, and thus involves more cost, time, and effort. As a panacea, GRA was introduced, in which several parameters are combined and optimized. GRA is used to unravel real problems consisting of limited data. It is usually used to estimate the properties of indefinite systems without black and white solutions. GRG is largely applied in optimization problems dealing with several parameters and responses [40,41]. Data preprocessing via GRA was executed on the responses (M_L , V_L , μ , and T_s). The reference sequence and deviation sequence (0–1) of the responses were computed using Equations (3) and (4), respectively. Figures 15 and 16 show the reference sequence and deviation sequence values, respectively, after the data pre-processing. The GRC for each value of the response was computed (Equation (5)). Ultimately, the mean of the GRCs was calculated to establish the GRG, and the calculated values were utilized to produce equivalent SNRs. A higher SNR is useful and indicates that the trials lie in proximity to the actual normalized magnitude of the GRG. Once the ranks were found (Figure 17), a GRG response table was contrived. From Figure 18, it is clear that the eleventh trial possessed the highest SNR. Therefore, the first rank was designated to the eleventh trial. The GRG of each parameter at the selected level was chosen and the average computed to obtain the mean GRG for each separate parameter, for example, parameter G at level 1 in the first, fourth, and seventh runs of the test. The concomitant GRG values from Table 8 were used for computation, as indicated in Equation (8).

Table 8. Response table for means of GRG.

Level	L (N)	G (mesh)	SD (m)	SS (ms^{-1})
1	0.6410	0.5136	0.6235	0.6514
2	0.6477	0.6322	0.6469	0.6261
3	0.6524	0.7955	0.6708	0.6637
Delta	0.0114	0.2819	0.0473	0.0376
Rank	4	1	2	3

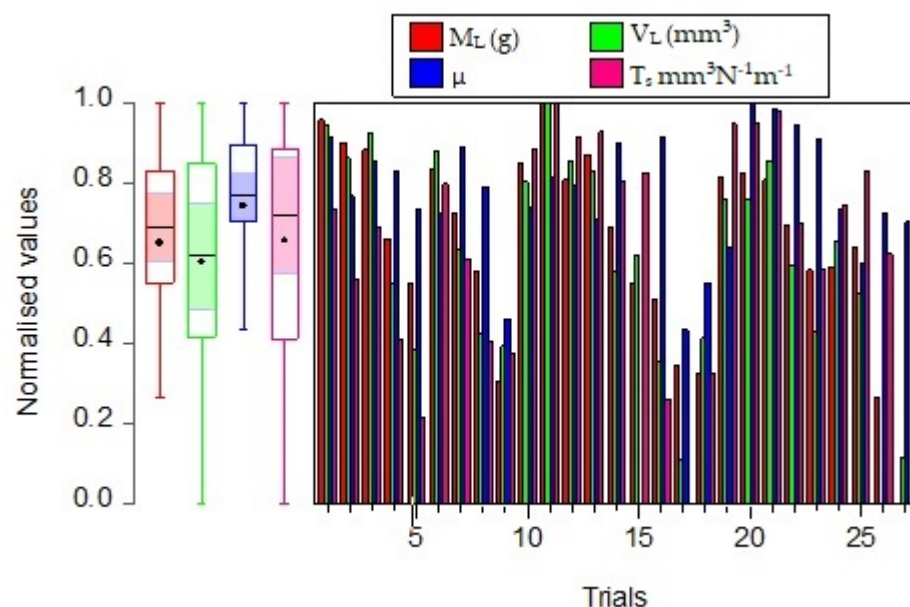


Figure 15. Reference sequence values for the L_{27} (3^4) hybrid-Taguchi OA.

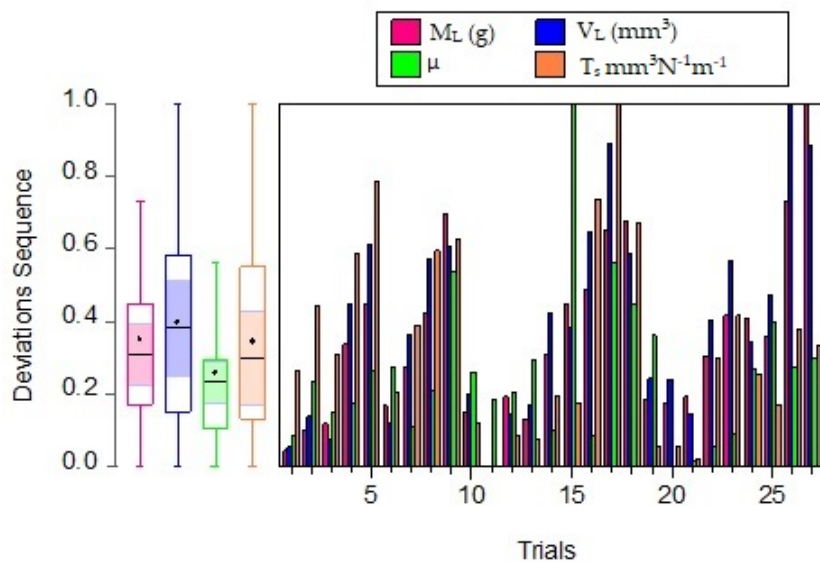


Figure 16. Deviation sequence for the L_{27} (3^4) hybrid Taguchi–OA. T_s ($\text{mm}^3\text{N}^{-1}\text{m}^{-1}$) μ .

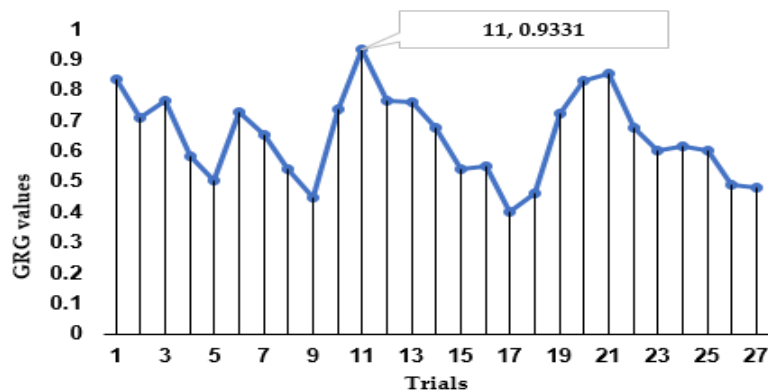


Figure 17. Graph showing the peak ranking of the trials of the GRG.

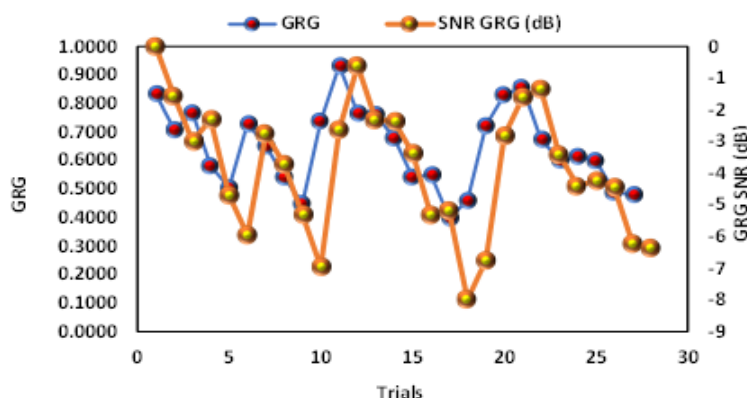


Figure 18. Plot of GRG versus SNRs.

The mean of the chosen GRGs was computed through the aforementioned method and put together to generate the response table (Table 8). The grades in Table 8 were utilized to serve as a measure between the comparability sequence and reference sequence of the GRA. Higher values for the mean GRGs exhibit a strong degree of correlation [42]. Hence, from Table 8, it is possible to achieve a combination of optimal parameters that maximizes the overall response. As observed in Table 8, the maximum GRG exists at L3, G1, SD3, and SS3. Therefore, to wrap it up, the optimal parameter settings for the useful abrasive tribological properties of PTFE-based composites are L at 9 N, G at 1000 mesh, sliding distance at 55 m,

and sliding speed at 0.14 ms^{-1} , coded as L3G1SD3SS3. The ANOVA results of the GRG revealed that grit size has the maximum percentage contribution of 94.56% upon GRG, succeeded by SS with 2.71%, SD with 2.18%, and load with a minimal contribution of 0.55%. This signifies that grit size is the most significant parameter that influences the abrasive wear property of PTFE-based composites.

3.5. Validation

After the identification of the optimal levels, the final phase in the GRA is the prediction and validation of the performance enhancement of the outputs. The predicted GRG was calculated as per Equation (7). Validation trials were performed to verify the results of the investigation. The optimized levels of M_L , V_L , μ , and T_s were found to be $8.5 \times 10^{-4} \text{ g}$, $4.1 \times 10^{-4} \text{ mm}^3$, 2.0×10^{-1} , and $1.5353 \times 10^{-6} \text{ mm}^3 \text{ N}^{-1} \text{ m}^{-1}$, respectively. It can also be implied from Table 9 that the findings of the validation stage are consistent with the computed values. In addition, an enhancement of 52% in the GRG was also achieved.

Table 9. Results of the validation test.

Optimal Parameter			
Initial Design Parameter	Prediction	Validation	
Level settings	L2G2SD3SS1	L3G1SD3SS3	L3G1SD3SS3
GRG	0.3988	0.8412	0.8311
Enhancement (%)		53	52

3.6. Performance Appraisal of the Artificial Intelligence Techniques

The GRG was predicted using hybrid models. The usefulness of the model was examined by comparing the predicted and the observed values. The purpose of using many physical and mathematical models is due to the important contribution offered by artificial intelligence and optimization techniques. Generally, physical-based and linear models are adopted for the prediction of the tribological behaviors of materials. These conventional techniques involve a lot of computational load, are time-consuming, and are unable to deal with the non-linearity intricacies of the tribological behaviors of materials such as PTFE matrix composites. By contrast, non-linear models based on AI can serve as a panacea to traditional models. The simulation process was performed in MATLAB 9.3 (R2020a). Figure 3 shows the bar plot of the raw data used as inputs to the models. The optimal structure of the SVR model was chosen via the trial-and-error approach. The model's prediction accuracies were appraised using the R^2 , R, MSE, RMSE, and MAPE of Equations (15)–(19), respectively, in both the training and testing phases.

Based upon the model inputs, the simulated outcomes in terms of the model appraisal metrics are depicted in Table 10. It was observed that the SVR model exhibited a poor training pattern following the appraisal measures. As a means of improving the training capability of the SVR model, optimization models, namely PSO and HHO, were added to the SVR model. Following the hybridization of the SVR model, its performance was found to increase. Moreover, when the hybrid models (SVR-PSO and SVR-HHO) are compared, different performances are observed (Table 10). Table 10 shows that the SVR-HHO model indicated the highest R^2 and R, but the lowest MSE, RMSE, and MAPE of 85%, 92%, 1%, 3%, and 3%, respectively, in predicting the GRG when compared with the SVR-PSO model. This shows that the model accurately learns the pattern of the data. Conclusively, the findings revealed that the predictive efficiency of the hybrid SVR-HHO model outshone that of the SVR-PSO and the SVR models for predicting the GRG. Additional investigation of the models was performed using radar plots, and is presented in Figure 19. It can be deciphered that $\text{SVR-HHO} > \text{SVR-PSO}$ were adequate enough to capture the best fitting for the GRG ($R^2 > 83\%$). Similarly, the numerical comparison of MSE showed that the SVR-HHO model with an MSE of 0.0014 is better than the SVR-PSO model with an MSE of 0.0031. The best predictive model reduced the error by 3%. Figure 20 showcases the scatter

plot between actual and predicted values of the SVR, SVR-PSO, and SVR-HHO models for GRG. The scatter plot gives an insight into the level of consistency between the predicted and actual GRG for the whole goodness of fit. It is clear from Figure 20 that the SVR-HHO model indicated better consistency between the actual and predicted GRG when compared with the SVR-PSO and SVR models.

Table 10. Findings of the appraisal of the single and hybrid models for predicting GRG.

Calibration					
Models	R ²	R	MSE	RMSE	MAPE
SVR	0.4736	0.6953	0.0082	0.0906	0.0978
SVR-PSO	0.6496	0.8100	0.0043	0.0657	0.0823
SVR-HHO	0.8470	0.9218	0.0009	0.0293	0.0291
Verification					
	R ²	R	MSE	RMSE	MAPE
SVR	0.8244	0.9080	0.0041	0.0637	0.0853
SVR-PSO	0.8498	0.9218	0.0031	0.0556	0.0546
SVR-HHO	0.8534	0.9238	0.0014	0.0368	0.0116

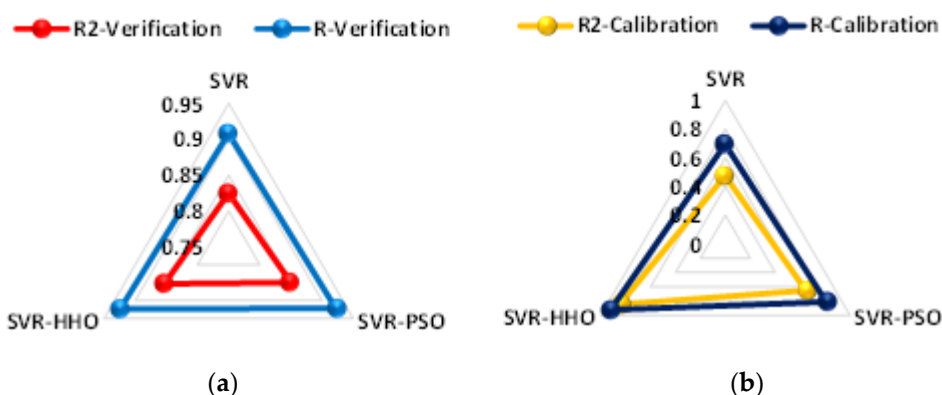


Figure 19. Radar plot for GRG in the (a) calibration and (b) verifications stages.

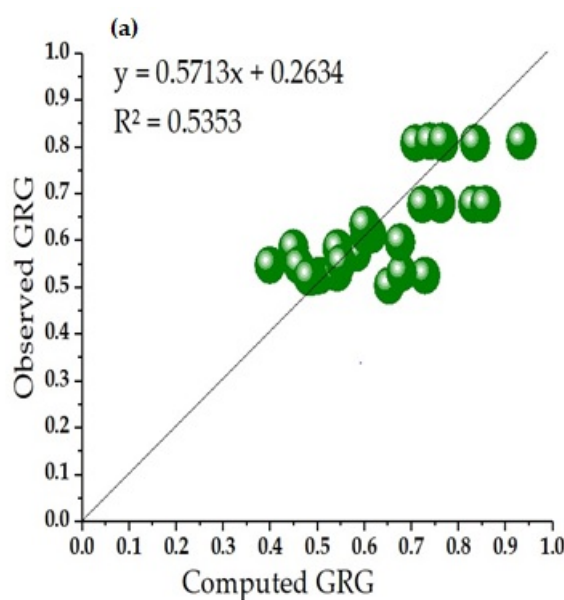


Figure 20. Cont.

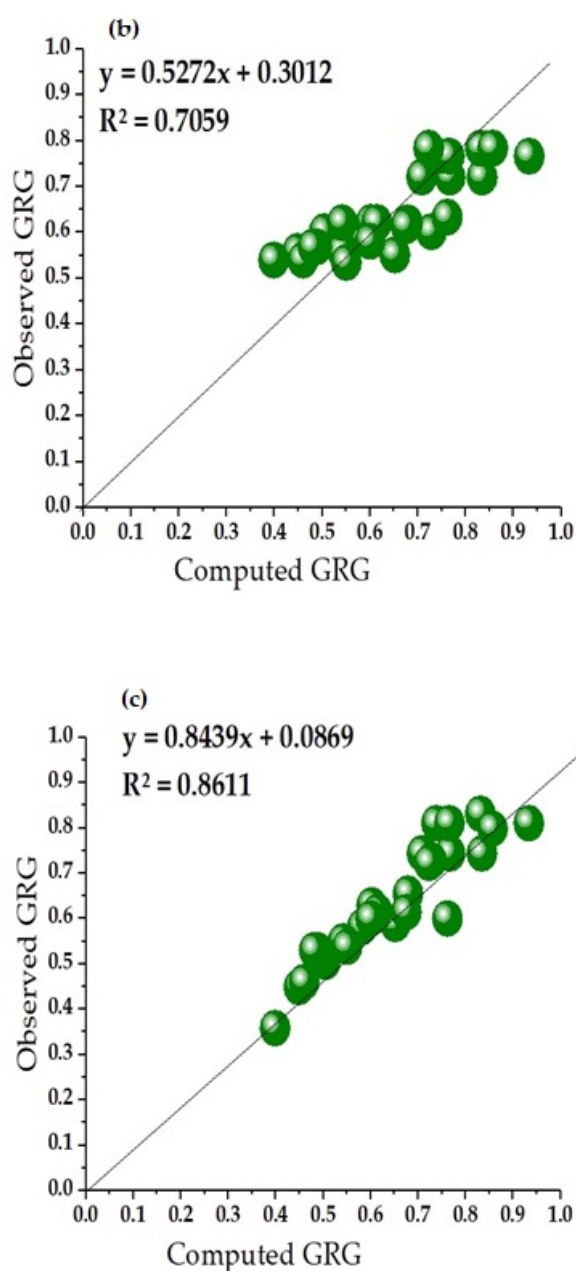


Figure 20. Scatter plot for (a) SVR, (b) SVR-PSO, and (c) SVR-HHO models for all datasets.

An overall comparison of the novel AI models in this study was carried out using a two-dimensional Taylor diagram, as depicted in Figure 21. The Taylor diagram describes and sums up many statistical metrics, such as RMSE, R, and standard deviation, between the actual and predicted values. This diagram can explain the goodness of fit of different techniques when compared with other models. Hence, this diagram can be visualized as a series of points against a polar plot. As noticed in Figure 21, the SVR model exhibited lower mimicking of the data pattern, with an R value = 47%. However, when the SVR-PSO and SVR-HHO models were compared, it was seen that their learning capability outperformed that of the SVR model by 16% and 22%, respectively. With respect to the prediction capability of the GRG, the performance of the SVR-HHO model was slightly higher than that of the SVR-PSO model by just 0.2%. These findings culminated in the conclusion that SVR-PSO and SVR-HHO models are sufficient in capturing the complex and non-linear trends of the GRG.

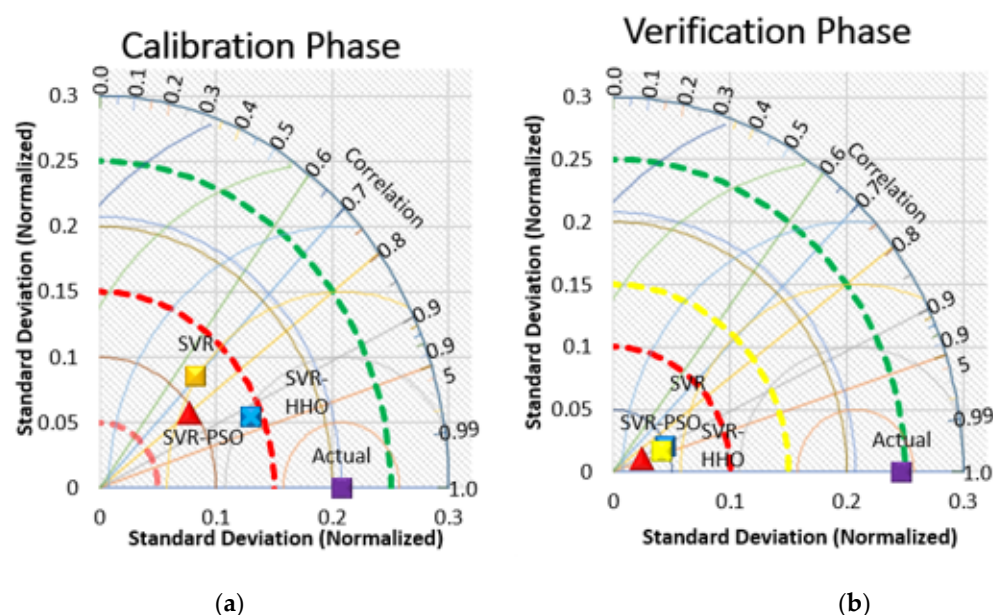


Figure 21. Taylor diagram for the models in the (a) calibration and (b) verification stages.

Nevertheless, taking into consideration the appraisal performance metrics, the simulated findings provided adequate ground for a high level of prediction superiority of all the artificial intelligence techniques in spite of the better predictive ability exhibited by the SVR technique.

4. Discussion

In Figure 7, it can be seen that increasing the load increased the mass loss of the materials. The ability of composite materials to resist wear relies on the composites forming adherent, uniform, and thin transfer film on the counter wheel [43,44]. The transfer film along the counter wheel stops the direct interaction between the materials (PTFE matrix composites) and metal counter wheel face, preventing abrasive action and hence leading to reduced mass loss. Therefore, the reason for the increase in mass loss due to an increase in the load is attributed to the high load breaking the tribolayer between the composites and the counterpart. Moreover, the decrease in the mass loss due to an increase in speed, distance, and grit size is related to the formation of an adherent, thin, and uniform tribolayer. The insignificant lower mass loss of the CF25 composite compared to the BF40 composite was connected to the carbon fiber's inherent properties. This finding tallies with [19,43,45]. The decrease in volume loss due to an increase in the sliding distance and speed is attributed to an increase in temperature at high speed, forming a layer preventing direct contact with the counter wheel face. The CF25 composite exhibited the best and worst volume loss at run 6 and 26, respectively. The minimum volume loss is related to the lower grit size, while the maximum was as a result of a higher grit size and the highly brittle nature of carbon fiber.

As noticed in Figure 9, the lowest μ was attained at 9 N. The reason for this is the formation tribolayer at the interacting state, as well as the temperature and visco-elastic-related behaviors of the PTFE matrix composites. This layer prevented the PTFE matrix composites from coming into direct contact with the abrasive surface, thus minimizing μ . Similar observations were made by [46]. The high μ at 6 N was perhaps due to the tearing of the transfer film at the contact region. This finding was contrary to the results obtained by [47]. High μ at 150 mesh is related to the high roughness of the SiC paper that offered a significant amount of resistance, while the low μ at 1000 mesh is attributed to the smoothness of the abrasive paper that offered little resistance to the samples—all due to the formation of the protective layer at the contact surface. The high friction due to an increase in the sliding distance is explained on the basis that the distance acted as a

lubricant to the rubbing surfaces. Thus, when the distance is increased, the lubrication is lost, thereby leading to excessive wear. The reason for the lower μ owing to an increase in the sliding speed is attributed to the adhesion between the matrix and the fibers as a result of the elevation in temperature. This is because when the sliding speed increases, the materials' strength is reduced, but their adhesion (tribolayer) is enhanced due to the elevated temperature. The low μ due to the increase in speed is related to the decrease in the contact time of the abrasives due to the high speed, thereby reducing the intensity of the tangential forces.

As presented in Figure 10, T_s decreased with an increase in the load, grit size, sliding distance, and sliding speed. The low T_s at high load (9 N) was because of the significant increase in the apparent contact area at high load, thereby leading to an increase in the contact area, permitting a large number of particles to meet at the interface and share the stress. This, in turn, reduced the abrasive tribological rate. The decrease in the tribological rate due to the increase in the abrasive size is related to clogging of the wear track with wear debris and a reduction in the cutting efficiency of the abrasives due to transfer. T_s reduction due to the increase in the sliding distance is attributed to the pull out or fracture of the abrasives as a result of the presence of tough carbon and bronze fibers. Additionally, wear debris is transferred to the counterface from the PTFE, causing reduced abrasion. Lower T_s due to increasing sliding is because the increase in speed increases the momentum transfer in the perpendicular direction, thus increasing the upward force upon the sample surface due to rotational inertia. Additionally, the travelling time is depreciated due to the increasing sliding speed. This minimizes wear debris generation, causing a reduced wear rate. Besides, at higher sliding speeds, plastic deformation becomes more difficult, causing less extensive damage compared to lower sliding speeds. Moreover, abrasive particle cracking increased at higher speeds, thereby decreasing the cutting efficiency of the abrasives and blunting the sharp edges of the abrasive particles.

The results of the single and multi-response optimization and ANOVA revealed different behaviors, implying that different tribological mechanisms might have been involved. In both the optimizations and ANOVA, grit size was the most influential parameter. This is attributed to the maximum inclination of the grit size compared to the load, distance, and speed. Similar results were obtained by Sahin [22]. From the confirmatory test, it was found that there was performance enhancement (52%) in the GRG over the initial design parameters. This improvement is explained by the fact that the GRA has added its sterling optimization features to those of the Taguchi technique, which cannot deal with multiple outcomes simultaneously. This confirms the validity of the Taguchi technique coupled with GRA for studying the abrasive tribological performance of PTFE matrix composites.

With respect to the prediction ability of the SVR, SVR-PSO, and SVR-HHO models, it was found that the SVR model was not good enough at calibrating and verifying the GRG of the PTFE matrix composites. The reason for the poor performance of the SVR model compared to its hybrids might be due to the highly complex and nonlinear nature of the data. Fundamentally, it should be considered that the promising prediction occurred in the course of the training phase, which is originally used to precisely measure the model based on known inputs and outputs. Nevertheless, the verification stage is significant in appraising the efficacy of the models, since it closely inspects the models' prediction efficiency based upon unknown magnitudes. This advantage is not enjoyed by the training phase of the SVR model. Consequently, a robust model should possess a determinate and balanced performance in both its training and testing stages. In general, the optimization algorithms showed promising ability when compared with a single model. The exceptional performance of the hybrid models is attributed to their ability to reduce errors and complexities. The slightly higher performance of the SVR-HHO model in comparison to the SVR-PSO model related to its cooperative mechanism and hunting behavior. Furthermore, the R values of the models were determined to be >80%, supporting the conclusions drawn by [38,48,49] that values >70% are considered acceptable. Consequently, the outcomes of

all of the optimization models are acceptable (Table 10). The predictive superiority of the HHO model over the others is in concordance with the results obtained by [50].

In spite of the availability of ample metaheuristic models, there is no particular model that can guarantee consistent optimal performance in addressing various types of issues. Yet, the latest research on unique population-based and nature-inspired optimization paradigm (HHO) models indicated better adequacy in establishing optimal solutions to problems in multi-objective forms. The statistical analysis outcomes and comparisons revealed that the SVR–HHO model yielded promising and often competitive outcomes compared with well-established metaheuristic models.

5. Conclusions

The principal objectives of this article were to perform multi-objective optimization and predict the grey relational grade (GRG) of polytetrafluoroethylene (PTFE) matrix composites via hybrid Taguchi–grey relational analysis (GRA) and support vector regression (SVR) models, respectively. The single optimization results revealed that mass loss and volume gave a similar optimal combination of parameters (L1G1SD1SS1), whereas the coefficient of friction and specific wear rate depicted different optimal combinations of parameter settings of L3G1SD1SS3 and L3G1SD3SS1, respectively. The analysis of variance (ANOVA) results showed that grit size was the most significant parameter influencing the tribological behaviors of polytetrafluoroethylene matrix composites. The results from the response table of the GRG revealed that the optimum parameters for the minimum tribological loss of PTFE matrix composites were the L3G1SS3SD3 combination. The ANOVA for the GRG indicated that grit size, with 94.56%, was the most significant parameter influencing the GRG of the PTFE matrix composites. The validation result depicted an enhancement of 52% in the GRG from 0.3988 (L2G2SD3SS1) for initial design parameters to 0.8311 for the optimal levels (L3G1SS3SD3). The prediction of the GRG using the hybrid models showed that the SVR–PSO and SVR–HHO models performed better than the single SVR model. Nevertheless, the SVR–HHO model predicted the GRG better than the SVR–PSO model, showing a lower prediction error of 1.16%, demonstrating its robustness and efficiency over the SVR–PSO hybrid artificial intelligence model with a prediction error of 5.46%.

Author Contributions: Conceptualization, methodology, formal analysis, writing and formal analysis, M.A.I.; Software analysis, S.I.A.; Resources, A.K.S. and M.M.; H.C. and M.A.S. supervision. All authors have read and agreed to the published version of the manuscript.

Funding: This research received no external funding.

Institutional Review Board Statement: Not applicable.

Informed Consent Statement: Not applicable.

Data Availability Statement: Not applicable.

Acknowledgments: Grateful to Kano University of Science and Technology, Wudil Kano State Nigeria, Kano State Scholarship Board, Kano State, Nigeria and Near East University, Nicosia, Cyprus.

Conflicts of Interest: The authors declare no conflict of interest.

References

1. Unal, H.; Sen, U.; Mimaroglu, A. Abrasive wear behaviour of polymeric materials. *Mater. Des.* **2005**, *26*, 705–710. [[CrossRef](#)]
2. Khedkar, E.I.; Negulescu, J.; Meletis, I. Sliding wear behavior of PTFE composites. *Wear* **2002**, *252*, 361–369. [[CrossRef](#)]
3. Bijwe, J.; Logani, C.M.; Tewari, U.S. Influence of fillers and fibre reinforcement on abrasive wear resistance of some polymeric composites. *Wear* **1990**, *138*, 77–92. [[CrossRef](#)]
4. Suresha, B.; Kumar, K.N.S. Investigations on mechanical and two-body abrasive wear behaviour of glass/carbon fabric reinforced vinyl ester composites. *Mater. Des.* **2009**, *30*, 2056–2060. [[CrossRef](#)]
5. Harsha, A.P.; Tewari, U.S. Abrasive wear resistance of glass fibre reinforced polysulfone composites. *Indian J. Eng. Mater. Sci.* **2002**, *9*, 203–208.

6. Unal, H.; Yetgin, S.H.; Mimaroglu, A.; Sumer, M. The effect of test parameters on friction and wear performance of PTFE and PTFE composites. *J. Reinf. Plast. Compos.* **2010**, *29*, 1978–1986. [[CrossRef](#)]
7. Şahin, Y.; Mirzayev, H. Wear characteristics of polymer-based composites. *Mech. Compos. Mater.* **2015**, *51*, 543–554. [[CrossRef](#)]
8. Kukureka, Y.K.; Hooke, S.N.; Rao, C.J.; Liao, M.; Chen, P. The effect of fibre reinforcement on the friction and wear of polyamide 66 under dry rolling–sliding contact. *Tribol. Int.* **1999**, *32*, 107–116. [[CrossRef](#)]
9. Ulas, M.; Altay, O.; Gurgenc, T.; Öznel, C. A new approach for prediction of the wear loss of PTA surface coatings using artificial neural network and basic, kernel-based, and weighted extreme learning machine. *Friction* **2019**, *8*, 1102–1116. [[CrossRef](#)]
10. He, R.; Chang, Q.; Huang, X.; Bo, J. Improved mechanical properties of carbon fiber reinforced PTFE composites by growing graphene oxide on carbon fiber surface. *Compos. Interfaces* **2018**, *25*, 995–1004. [[CrossRef](#)]
11. Suh, J.; Bae, D. Mechanical properties of polytetrafluoroethylene composites reinforced with graphene nanoplatelets by solid-state processing. *Compos. Part B Eng.* **2016**, *95*, 317–323. [[CrossRef](#)]
12. Shipway, N.K.; Ngao, P.H. Microscale abrasive wear of polymeric materials. *Wear* **2003**, *255*, 742–750. [[CrossRef](#)]
13. Ravi Kumar, B.N.; Suresha, B.; Venkataramareddy, M. Effect of particulate fillers on mechanical and abrasive wear behaviour of polyamide 66/polypropylene nanocomposites. *Mater. Des.* **2009**, *30*, 3852–3858. [[CrossRef](#)]
14. Liu, J.; Ren, C.; Tong, L.Q. Abrasive wear behavior of particle reinforced ultrahigh molecular weight polyethylene composites. *Wear* **1999**, *225*, 199–204. [[CrossRef](#)]
15. Yousif, B.F.; Nirmal, U.; Wong, K.J. Three-body abrasion on wear and frictional performance of treated betelnut fibre reinforced epoxy (T-BFRE) composite. *Mater. Des.* **2010**, *31*, 4514–4521. [[CrossRef](#)]
16. Montgomery, C.D. *Design and Analysis of Experiments*, 5th ed.; John Wiley & Sons: New York, NY, USA, 2001.
17. Sudarshan, N.; Varadarajan, R.K.; Rajendra, Y.S. Investigation of the abrasive wear behavior of graphite filled carbon fabric reinforced epoxy composite—A Taguchi approach. *Int. J. Mech. Eng. Technol.* **2013**, *4*, 101–108.
18. Ramesh., B.N.; Suresha, B. Optimization of tribological parameters in abrasive wear mode of carbon-epoxy hybrid composites. *Mater. Des.* **2014**, *59*, 38–49. [[CrossRef](#)]
19. Basavarajappa, J.P.; Arun, S.; Davim, K.V. Effect of filler materials on dry sliding wear behavior of polymer matrix composites—A Taguchi approach. *J. Miner. Mater. Charact. Eng.* **2009**, *8*, 379–391. [[CrossRef](#)]
20. Pogosian, A.K.; Cho Bahadur, S. Friction and wear studies using Taguchi method on polyphenylene sulfide filled with a complex mixture of MoS₂, Al₂O₃, and other compounds. *Wear* **2005**, *258*, 1825–1835.
21. Chauhan, S.R.; Thakur, S. Effects of particle size, particle loading and sliding distance on the friction and wear properties of cenosphere particulate filled vinyl ester composites. *Mater. Des.* **2013**, *51*, 398–408. [[CrossRef](#)]
22. Şahin, Y. Analysis of abrasive wear behavior of PTFE composite using Taguchi’s technique. *Cogent Eng.* **2015**, *1*, 1–15. [[CrossRef](#)]
23. Sudarshan, R.K. Modelling and analysis of abrasive wear performance of glass epoxy composites using Taguchi approach. *Int. J. Miner. Metall. Mater. Sci. Eng.* **2013**, *3*, 19–28.
24. Darshan, S.M.; Suresha, B.; Jamadar, I.M. Optimization of abrasive wear parameters of halloysite nanotubes reinforced silk/basalt hybridepoxy composites using Taguchi Approach. *Tribol. Ind.* **2021**, *in press*.
25. Dharmalingam, S.; Subramanian, R.; Kok, M. Optimization of abrasive wear performance in aluminium hybrid metal matrix composites using Taguchi-grey relational analysis. *Proc. Inst. Mech. Eng. Part J J. Eng. Tribol.* **2013**, *227*, 749–760. [[CrossRef](#)]
26. Sylajakumari, P.A.; Ramakrishnasamy, R. Taguchi grey relational analysis for multi-response optimization of wear in co-continuous composite. *Materials* **2018**, *11*, 1–17.
27. Saravanan, K.G.; Thanigaivelan, R. Optimisation of laser parameters and dimple geometry using PCA-coupled GRG. *Stroj. Vestn./J. Mech. Eng.* **2021**, *in press*. [[CrossRef](#)]
28. Velten, K.; Reinicke, R.; Friedrich, K. Wear volume prediction with artificial neural networks. *Tribol. Int.* **2000**, *33*, 731–736. [[CrossRef](#)]
29. Zhang, Z.; Friedrich, K.; Velten, K. Prediction on tribological properties of short fibre composites using artificial neural networks. *Wear* **2002**, *252*, 668–675. [[CrossRef](#)]
30. Jiang, Z.; Zhang, Z.; Friedrich, K. Prediction on wear properties of polymer composites with artificial neural networks. *Compos. Sci. Technol.* **2007**, *67*, 168–176. [[CrossRef](#)]
31. Jiang, Z.; Gyurova, L.; Zhang, Z.; Friedrich, K.; Schlarb, A.K. Neural network based prediction on mechanical and wear properties of short fibers reinforced polyamide composites. *Mater. Des.* **2008**, *29*, 628–637. [[CrossRef](#)]
32. Haghigat Mesbahi, A.; Semnani, D.; Nouri Khorasani, S. Performance prediction of a specific wear rate in epoxy nanocomposites with various composition content of polytetrafluoroethylene (PTFE), graphite, short carbon fibers (CF) and nano-TiO₂ using adaptive neuro-fuzzy inference system (ANFIS). *Compos. Part B Eng.* **2012**, *43*, 549–558. [[CrossRef](#)]
33. Ray, S. A comparative analysis of the abrasion wear characteristics of industrial wastes filled glass/polyester composites based on the design of experiment and neural network. *Polym. Compos. Polym.* **2020**, *42*, 424–438. [[CrossRef](#)]
34. Dutta, S.; Pal, S.K.; Sen, R. On-machine tool prediction of flank wear from machined surface images using texture analyses and support vector regression. *Precis. Eng.* **2016**, *43*, 34–42. [[CrossRef](#)]
35. Bhattacharyya, P.; Sanadhya, S.K. Support vector regression based tool wear assessment in face milling. *Proc. IEEE Int. Conf. Ind. Technol.* **2006**, 2468–2473.
36. Kalantary, S.; Jahani, A.; Pourbabaki, R.; Beigzadeh, Z. Application of ANN modeling techniques in the prediction of the diameter of PCL/gelatin nanofibers in environmental and medical studies. *RSC Adv.* **2019**, *9*, 24858–24874. [[CrossRef](#)]

37. Pachuri, V.S.; Sunjay, S.; Om Prakash, V.; Bhuvnesh, B.; Tarun, K.; Sharma, N. Prediction and optimization of abrasive wear loss of ultrahigh strength martensitic steel using response surface methodology, Harris Hawk and artificial neural network. *Int. J. Syst. Assur. Eng. Manag.* **2021**, *6*, 1–16.
38. Musa, B.; Yimen, N.; Abba, S.I.; Adun, H.H. Multi-state load demand forecasting using hybridized support vector regression integrated with optimal design of off-grid energy systems—A metaheuristic approach. *Proceses* **2021**, *9*, 1166. [[CrossRef](#)]
39. Abba, S.I.; Bara'u, G.N.; Abdulazeez, R.; Bashir, M.; Naseer, Y.; Kawu, S.J.; Lawan, S.M.; Mustafa, D. Emerging Harris Hawks Optimization based load demand forecasting and optimal sizing of stand-alone hybrid renewable energy systems—A case study of Kano and Abuja, Nigeria. *Results Eng.* **2021**, *12*, 100260. [[CrossRef](#)]
40. Zou, S.Y.; Huang, R.; Chi, M.C.; Hsu, H.M. Factors affecting the effectiveness of inorganic silicate sealer materials through multi-quality characteristics. *Materials* **2013**, *6*, 1204. [[CrossRef](#)]
41. Kasemsiri, P.; Dulsang, P.; Pongsa, N.; Hiziroglu, U.; Chindaprasit, S. Optimization of biodegradable foam composites from cassava starch, oil palm fibre, chitosan and palm oil using Taguchi method and grey relational analysis. *J. Polym. Environ.* **2017**, *25*, 78–390. [[CrossRef](#)]
42. Wojciechowski, P.; Maruda, S.; Krolczyk, R.W.; Nieslony, G.M. Application of signal noise ratio and grey relational analysis to minimize forces and vibrations during precise ball end milling. *Precis. Eng.* **2018**, *51*, 582–5596. [[CrossRef](#)]
43. Bahadur, C.; Sunkara, S. Effect of transfer film structure, composition and bonding on the tribological behavior of polyphenylene sulfide filled with nano particles of TiO₂, ZnO, CuO and SiC. *Wear* **2005**, *258*, 1411–1421. [[CrossRef](#)]
44. Schwartz, C.J.; Bahadur, S. The role of filler deformability, filler–polymer bonding, and counterface material on the tribological behavior of polyphenylene sulfide (PPS). *Wear* **2001**, *251*, 1532–1540. [[CrossRef](#)]
45. Chand, S.; Naik, N.; Neogi, A. Three-body abrasive wear of short glass fibre polyester composite. *Wear* **2000**, *242*, 38–46. [[CrossRef](#)]
46. Chowdhury, M.A.; Nuruzzaman, D.M.; Roy, B.K.; Samad, S.; Sarker, R.; Rezwan, A.H.M. Experimental Investigation of Friction Coefficient and Wear Rate of Composite Materials Sliding Against Smooth and Rough Mild Steel Counterfaces Tribology in Industry. *Tribol. Ind.* **2013**, *35*, 286–292.
47. Gunes, I.; Uygunoğlu, T.; Çelik, A.G. Tribological properties of fly ash blended polymer composites. *Matéria* **2021**, *26*, 1–11. [[CrossRef](#)]
48. LeGates, D.R.; McCabe, G.J. Evaluating the use of ‘goodness-of-fit’ Measures in hydrologic and hydroclimatic model validation. *Water Resour. Res.* **1999**, *35*, 233–241. [[CrossRef](#)]
49. Moriasi, T.L.; Arnold, D.N.; Van Liew, J.G.; Bingner, M.W.; Harmel, R.L.; Veith, R.D. Model evaluation guidelines for systematic quantification of accuracy in watershed simulations. *Trans. ASABE* **2007**, *50*, 885–900. [[CrossRef](#)]
50. Yu, S.B.; Kim, J.; Rhee, C.H. The comparison of lately proposed Harris Hawks optimization and Jaya optimization in solving directional overcurrent relays coordination problem. *Complexity* **2020**, *3*, 3807653. [[CrossRef](#)]